https://doi.org/10.1016/j.ijmultiphaseflow.2019.05.002

On the role of liquid viscosity in affecting droplet spreading on a smooth solid surface

Mengxiao Qin[1], Chenglong Tang[1]*, Shangqing Tong[1], Peng Zhang[2]*, and Zuohua Huang[1]

1. State Key Laboratory of Multiphase Flow in Power Engineering, Xi'an Jiaotong University, Xi'an, 710049, China

2. Department of Mechanical Engineering, The Hong Kong Polytechnic University, Hung Hom, Kowloon, Hong Kong

Abstract:

The role of liquid viscosity on droplet spreading behavior upon impacting on a smooth stainless steel surface has been experimentally investigated. Results show the droplet spreading dynamics with increasing viscosity (characterized by the Ohnesorge number, *Oh*) exhibits complex dependence on the impact inertia (characterized by Weber number, *We*). Specifically, for a small impact inertia (*We*<30), the droplet oscillates in the vertical direction around the maximum height H_a. The non-dimensional maximum diameter β_{max} first increases and then decreases with increasing *Oh*, and this non-monotonic phenomenon has not been reported previously. For an intermediate impact inertia (60<*We*<240), the droplet has no oscillation after it spreads to β_{max}, and it has the form of a rim-bounded lamella. Although β_{max} shows a monotonic decrease with increasing *Oh*, some unsmooth disturbance around the rim occurs only at intermediate *Oh*. For a higher impact inertia (*We*>240), droplet splashing emerges and then vanishes with increasing *Oh*, although β_{max} still decreases monotonically. All the observed phenomena imply that liquid viscosity may have a dual role in affecting the droplet spreading, which previous models of β_{max} do not take into account.

Keywords: Droplet impact; maximum spreading diameter; non-monotonic dependence; viscosity effect.

*Corresponding authors:

Chenglong Tang, Professor,

State Key Laboratory of Multiphase Flows in Power Engineering，

Xi'an Jiaotong University, Xi'an, 710049, People's Republic of China

Tel: 86-29-8266-5075, Fax: 86-29-8266-8789

Email: chenglongtang@mail.xjtu.edu.cn

Peng Zhang, Associate Professor,

Department of Mechanical Engineering,

The Hong Kong Polytechnic University, Hung Hom, Kowloon, Hong Kong

Tel: (852)2766-6664, Fax: (852)2365-4703

Email: pengzhang.zhang@polyu.edu.hk

1. Introduction

The impact of a single droplet on a solid surface or a thin-film is frequently observed in nature and industry processes, such as the aerosol generation from raindrops hitting soil (Joung and Buie, 2015), the blade erosion by high inertia droplet impact on steam turbines (Zhang et al., 2017), the extraction of useful information by police experts from bloodstains (Hulse-Smith et al., 2005; Smith et al., 2018), droplet splashing blemishes ink-jet printing (Martin et al., 2008). As for combustion engines, the impact of fuel droplets on the intake port, back of the intake valve, or even combustion chamber to form a thin liquid film is inevitable because of the limited space for mixture formation. Such a film deposit reduces the near wall fuel evaporation rate, especially at cold start condition, and ultimately increases the emission of unburned hydrocarbon and soot particles.

The droplet-wall impact outcome and spreading phenomenon are expected to be influenced by the properties of droplets (density ρ, viscosity μ, surface tension σ, droplet diameter D_0, and velocity U_0), the wall conditions (cold/heated, dry/wet, contact angle, roughness, etc.), and the surrounding gas (pressure, molecular weight, etc.). Weber number ($We=\rho D_0 U_0^2/\sigma$) and Ohnesorge number ($Oh=\mu/(\rho D_0 \sigma)^{1/2}$), which respectively measures the ratio of inertia and viscous force over the surface tension force, are typically used to describe the complex impact outcomes such as spreading and rebound (without secondary droplets), prompt, fingering, corona and thin sheet splashing (with secondary droplets), as reviewed in a few previous papers (Josserand and Thoroddsen, 2016; Moreira et al., 2010; Rioboo et al., 2001; Yarin, 2006).

For droplet impact on dry and cold surfaces, as far as the spreading outcome being concerned, several experimental and theoretical investigations have been conducted, in terms of descriptions of the spreading phenomenon (Bayer and Megaridis, 2006; Laan et al., 2014; Lee et al., 2016a; Lee et al., 2016b; Pasandideh‐Fard et al., 1996; Seo et al., 2015; Ukiwe and Kwok, 2005; Vadillo et al., 2009) and the evolution of the normalized spreading diameter β (Bayer and Megaridis, 2006; Laan et al.,

2014; Lee et al., 2016a; Pasandideh‐Fard et al., 1996; Vadillo et al., 2009), empirical or theoretical models of the maximum spreading diameter β_{max} (Bayer and Megaridis, 2006; Laan et al., 2014; Lee et al., 2016a; Roisman, 2009; Wildeman et al., 2016) and their parametric dependence (Josserand and Thoroddsen, 2016; Moreira et al., 2010; Yarin, 2006).

Specifically, the spreading process upon impact is usually divided into several stages, namely the *kinematic*, *spreading*, *relaxation and equilibrium* stage (Rioboo et al., 2002). For the *kinematic* stage (β<1), the evolution of β is barely influenced by surface roughness, *We* or *Oh*, and simply evolves with the square root of the normalized time τ.

In the subsequent *spreading* stage ($1<\beta<\beta_{max}$), various parameters begin to affect the spreading dynamics in terms of the droplet deformation and the evolution of β. For instance, the droplet typically spreads out in a rim-bounded lamella, and β increases with τ. Generally, larger *We* and smaller *Oh* result in the acceleration of β because of the higher inertia and smaller viscous dissipation (Lee et al., 2016b; Tang et al., 2017; Vadillo et al., 2009). Influence of wettability on the evolution of β was only observed for very hydrophobic surfaces during the final stage of spreading (Rioboo et al., 2002). Surface roughness was found to slightly reduce the evolution of β (Tang et al., 2017) and the number of fingers (Range and Feuillebois, 1998). Lower ambient gas pressure delays the appearance of the thin sheet and suppresses fingering (Xu et al., 2005). The development of fingers during the spreading and the model prediction of the number of fingers were studied in the context of Rayleigh-Taylor instability (Allen, 1975; Bhola and Chandra, 1999; Thoroddsen and Sakakibara, 1998; Vu et al., 2011; Yarin, 2006). These studies investigated the occurrence of thin sheet and the mechanism of such instability at the rim of the droplet during spreading.

After reaching β_{max}, the droplet may contract back (β decreases) or its periphery is fixed at β_{max}. Excess kinetic energy keeps on dissipating through *relaxation* and finally reaches *equilibrium.* Banks et al. (2014) investigated the effect of droplet impact velocity, viscosity and solid surfaces on the

oscillation frequency and initial amplitude. They found that the increase of impact velocity restricts the oscillation and that the effect of viscosity on the oscillation frequency and amplitude depends on the surface material. Lin et al. (2018) analyzed the oscillation with the damped harmonic system and interpreted the effects of liquid viscosity and surface wettability on the oscillation by scaling analyses.

Different models have been proposed to predict β_{max}. The scaling law of β_{max}~(Re^2Oh) (Bayer and Megaridis, 2006; Scheller and Bousfield, 1995; Seo et al., 2015) and the Padé approximation (Laan et al., 2014; Lee et al., 2016b) were widely used. Roisman (2009) developed an analytical self-similar solution which satisfies the Navier-Stokes equation. Models based on energy conservation, which consider the energy conversion from kinetic energy to surface energy and to viscous dissipation, mainly focus on the estimation of viscous dissipation during the droplet spreading (Chandra and Avedisian, 1991; Pasandideh‐Fard et al., 1996; Ukiwe and Kwok, 2005; Vadillo et al., 2009). Wildeman et al. (2016) found that approximately one-half of the initial kinetic energy is transformed into surface energy for high impact velocities and free-slip surface. As for no-slip surface condition, the head loss can be added into the total dissipation as one-half of the initial kinetic energy. The prediction of viscous dissipation during the spreading plays vital role in the models based on energy conservation, and the time when the droplet reaches its maximum spreading diameter t_{max} has been extensively studied and refined by different approach (Chandra and Avedisian, 1991; Gao et al., 2018; Lee et al., 2016a; Pasandideh‐Fard et al., 1996).

Viscosity is an important and fundamental element in fluid mechanics, which also significantly influences the spreading process and splashing patterns. Xu et al. (2005) found the non-monotonic effect of viscosity on the splashing threshold pressure, but the effect of viscosity on spreading has not been investigated sufficiently. In addition, most of the previous work were focused on the relatively high impact inertia, and show that increasing viscosity suppresses the evolution of β. The first objective of this work is then to systematically investigate the effect of viscosity on the impact behavior and the evolution of the spreading diameter, over a wide range of *We*. We will show that less viscous liquid

does not always promote the evolution of β. In addition, the previous empirical or theoretical correlations on β_{max} are based on the experimental data from various pure liquids with simultaneously varying surface tension and viscosity, which make it hard to decouple the influence of viscosity from that of surface tension. Thus the second objective of this work is to provide a mapping of β_{max} with a wide range of viscosity for different impact inertia, but with negligible change of surface tension. Finally, the previous models on β_{max} will be compared with the present experimental data to evaluate their validity range, and theoretical considerations for future modelling will be discussed. In the following text, the experimentation will be specified in Section 2, followed by the phenomenological descriptions of droplet impact with emphasis on the viscosity effects, in Section 3. Quantitative description of the viscosity effects on the spreading behavior will be discussed in Section 4, and the empirical correlations on β_{max} will be compared and analyzed in Section 5.

2. Experimental specifications

2.1 High-speed Imaging System

The experimental system used in the present study has been described in great detail in our previous work (Tang et al., 2017) and will be briefly summarized as follows. The droplet impacting process is recorded by a phantom V611 high-speed camera attached by a long focus microscope, operating at 10,000 fps with a 1104×504 pixel resolution. The camera is tilted by 15° to get information about the horizontal surface morphology, such as the fingering disturbance and thin sheet. The vertical velocity is corrected with the cosine value of 15°. The droplet is released from different height, resulting in variation of the impacting velocities ranging from 0.5 m/s to 4.1 m/s. The surface used in the present experiment is smooth (R_a=0.025μm) stainless steel.

2.2 Characterization of droplet

The experiments were conducted with different glycerol solutions with viscosity μ varying from 1.6 mPa·s to 25.08 mPa·s. Other typical properties of the liquids are presented in Table 1. Figure 1 presents the non-dimensional surface tension, viscosity and density of glycerol solutions. The density and surface tension of these glycerol solutions are nearly constant, and the viscosity changes more than one order of magnitude. Two non-dimensional parameters will be used to describe the droplet dynamics, namely the Weber number $We=\rho D_0 U_0^2/\sigma$ and the Ohnesorge number $Oh=\mu/(\rho\sigma D_0)^{1/2}$. The estimated maximum error in the droplet shape is about 2 pixels (equivalent to 0.02 mm with a 0.01 mm/pixel spatial resolution). Consequently, the uncertainty of D_0 is about ± 0.04 mm, and that of U_0 is less than 2%. As a result, the relative error of the Weber number, $\Delta We/We = \Delta D_0/D_0 + 2\Delta U/U$, is less than 6%. Correspondingly, non-dimensional maximum spreading diameter is $\beta_{max}=D_{max}/D_0$ and the non-dimensional time is $\tau = tU_0/D_0$.

The test ranges of *Oh* and *We* are presented in Figure 2. As the cases of the least and the most viscous liquids, the 10% and 70% glycerol solutions did not result in droplet splashing until We=726 (roughly the maximum *We* that could be achieved in the experiment). For other glycerol solutions, splashing is observed when *We* is sufficiently large.

3. Phenomenological descriptions on viscosity effects

In our previous work (Tang et al., 2017), we have identified different stages of spreading upon impact of a droplet on stainless steel solid surface that characterize the spreading behavior, namely the *kinematic*, *spreading*, *relaxation* and *equilibrium* stage, with emphasis on the effect of surface roughness. In this work, we focus on the effect of viscosity on the phenomenological impact behavior, during those identified stages, on a smooth solid surface at small, intermediate and large impact inertia cases.

3.1 Representative cases at a small Weber number

Figure 3 shows the images of droplet impact process at a relatively low *We* (*We*≈ 13). Both dimensional and non-dimensional spreading time are presented in the figure.

At the *kinematic* stage (β<1), there is barely a difference in droplets with varied *Oh*. At 0.5ms, the top of the droplet keeps spherical and the bottom of the droplet has already contacted with the surface and formed a liquid film.

At the *spreading* stage (1<β<β_{max}), there are some horizontal ripples (capillary waves) that propagate from the wall to the top of the droplet, as shown in the images at 2ms. This kind of capillary wave propagation is consistent with the experimental observation by Bayer and Megaridis (2006). In addition, at this *spreading* stage, the viscosity begins to play a role in the spreading process. At different *Oh*, the droplet spreads at different velocity and eventually results in a quite different β_{max}. The time instant when the droplet reaches β_{max} is defined as t_{max} and marked in the figure. Interestingly, β_{max} first increases and then decreases with increasing *Oh*; the same non-monotonic variation occurs for t_{max}.

At the *relaxation* stage (t>t_{max}), droplet oscillation is observed. Part of the rim returns to the center of the droplet after reaching β_{max}, and then spreads to the rim again with a little change in the horizontal direction but with a remarkable change of the height of droplet center in the vertical direction. This behavior is evidently different from a simple interface retraction. The droplet at *Oh*=0.0038 reaches the oscillating apex at 11.3ms, 23.6ms, 35.3ms and 43.5ms, respectively. The time to reach the oscillating apex for the first time is defined as t_a and marked in the figure, the height of the apex at t_a is defined as H_a. It is seen that t_a first increases and then decreases with increasing *Oh,* also indicating the non-monotonic effect of viscosity. At final stage when all the kinetic energy is dissipated, the droplet exhibits as a spherical cap shape. Further quantitative analysis and underlying physics will be discussed in detail in Section 4.

3.2 Representative cases at intermediate Weber numbers

Figure 4 shows images of droplet impact process with varied viscosity at $We \approx 60$. Droplet oscillation is significantly suppressed and is only observed at a relatively high *Oh* (*Oh*=0.0592). Images of $\beta < 1$ are not shown since at these *We*, only one or two images are captured during the *kinematic* stage. During the *spreading* stage, as it is different from the cases at $We \approx 13$, no propagating ripples are observed for these cases. In addition, both t_{max} and β_{max} change monotonically with the increase of *Oh*. Viscosity significantly reduces t_{max} (correspondingly, τ_{max}) from 4.9ms(2.4) at *Oh*=0.0038 to 2.8ms(1.4) at *Oh*=0.0592. During the spreading, the rim of the droplet remains smooth with no visible disturbance. The thickness of the rim increases with the increase of *Oh* (de Ruiter et al., 2010), but this is hardly visible in this work because of the 15° tilted camera view. At the final *equilibrium* stage, unlike the small *We* cases, the droplet does not show any oscillation.

To further investigate the impact characteristics at intermediate *We*, Figure 5 shows the impact images at $We \approx 200$. At 0.5ms, the droplet keeps spherical away from the surface and its impact interface already forms a liquid film. The droplet oscillation is not visible at this *We*; the rim of the droplet becomes thinner, which is consistent with the previous observation (Wang et al., 2018). Compared with the cases at $We \approx 60$, both t_{max} and τ_{max} are reduced at $We \approx 200$. It still takes shorter time for glycerol solution with higher viscosity to reach smaller β_{max}.

Another non-monotonic phenomenon with the increase of *Oh* is observed. At *Oh*=0.0287, a thin sheet, which is much thinner than the rim and is levitated from the surface appears between the rim and inner droplet at 0.5ms and then leads to an instability at 1.5ms. This observation is consistent with that in the previous study (Driscoll and Nagel, 2011). However, such a thin sheet is absent at higher *Oh* (*Oh*=0.0592), and the rim tends to be stable again. Partially enlarged images is presented as Figure 5b for better comparison. Similar non-monotonic phenomenon of viscosity was observed in the previous study of Vu et al. (2011), where they compared the splashing characteristics of glycerol solution droplets with different viscosity.

3.3 Representative cases at high Weber number

The presence of a thin sheet is more pronounced at higher *We* as presented in Figure 6 for $We\approx$ 400. At 0.3ms, which is the very beginning of spreading, no thin sheet is observed at *Oh*=0.0038. At *Oh*=0.0070, the edge of the droplet has a distinct thin-sheet inclined to the wall, with a finger protrusion. The thin sheet becomes more pronounced at *Oh*=0.0166 but with a smaller finger-like protrusion. At *Oh*=0.0287, the less obvious thin sheet is almost attached to the solid surface, and it is difficult to observe at *Oh*=0.0592.

At 0.4ms, both the droplet and the thin sheet keep outspreading, and there is still no thin-sheet or any disturbance at *Oh*=0.0038. The thin sheet at *Oh*=0.0070 breaks up and produces many smaller secondary droplets, while it still remains stable and does not break at *Oh*=0.0166, *Oh*=0.0287 and *Oh*=0.0592.

The droplets at *Oh*=0.0166 and *Oh*=0.0287 splash at 0.8ms. Although the splashing patterns and the influence of viscosity on the splashing dynamics are not the focus of this work, we do need to mention the splashing outcome because it is only observed at intermediate *Oh* numbers. In general, the result of the droplet impact changes from deposition (*Oh*=0.0038) to thin sheet splashing (*Oh*=0.0070, 0.0166, 0.0287), and then to deposition again (*Oh*=0.0592).

Droplet splashing is a complex phenomenon that has not been fully understood (Josserand and Thoroddsen, 2016). The classical splashing threshold (Mundo et al., 1995; Stow and Hadfield, 1981) is given by $K_{cr}=WeRe^{1/2}>3000$, which can be rewritten by $K_{cr}=We^{5/4}Oh^{-1/2}$ by using the relation $Re=We^{1/2}Oh^{-1}$. Considering *Oh*=0.0038, 0.0070, 0.0166, 0.0287 and 0.0592 in the present experimental investigation, we can estimate the corresponding threshold $We_{cr}=K_{cr}^{4/5}Oh^{2/5}$ for observing droplet splashing by are 65, 83, 117, 146 and 195, respectively. This estimation is roughly consistent with the observation that the most viscous liquid (*Oh*=0.0592) results in deposition. However, there is no splashing for the droplet with smallest viscosity (*Oh*=0.0038), implying that the critical Weber number decreases and then increases with increasing *Oh*. A number of power laws in the form of $K_{cr}=\mathrm{A}We^{a}Oh^{b}$

were summarized in the review (Moreira et al., 2010), but none of them implies the non-monotonic emergence of droplet splashing with increasing *Oh*. A possible explanation is that the existing scaling laws do not consider the different splashing types (e.g. prompt and thin sheet splashing) for different droplet viscosity. Another possible explanation to the present observation is proposed as follows.

The earlier work of Xu et al. (2005) has reported that "a more viscous liquid splashes more easily than a less viscous one". They attributed this to the decreased capillary pressure on the spreading liquid layer with increasing liquid viscosity, as $\Sigma_L = \sigma/d = \sigma/\sqrt{\nu_L t}$. The range of Ohnesorge number (*Oh*=0.0024-0.0083) in which they observed the phenomenon is consistent with that in the present study (*Oh*=0.0038-0.0103). Furthermore, we note that further increasing liquid viscosity would eventually suppress the splashing by stabilizing the growing unstable waves (Matas, 2015; Naraigh and Spelt, 2018). Consequently, visible splashing is not observed for the case of *We*=400 and *Oh*=0.0592 and may appear at higher *We*. Further quantitative analyses for the appearance and disappearance of splashing and for the transition from prompt to thin sheet splashing with increasing *Oh* are beyond the scope of the present study and certainly deserve more future efforts.

4. Viscosity effects on spreading dynamics

4.1 Evolution of spreading diameter and center height

Figure 7 shows the evolution of β at three representative Weber numbers (13, 200 and 400) and various *Oh*. At the *kinematic* phase (β<1), β increases as approximately $\beta \sim 3\tau^{0.57}$, which is consistent with the previous observation of Rioboo et al. (2002). There is almost no difference in β among various *Oh*, rendering a seemingly "*Oh*-independent" stage where the spreading process can be completely described by the impact velocity U_0 and initial diameter D_0. This phenomenon can be understood by recognizing that the droplet impact velocity has not been substantially decelerated at the early stage, so the characteristic velocity is approximately equal to U_0 and *Re* can be roughly estimated as $Re=We^{1/2}Oh$ which is about $O(10^2)$-$O(10^4)$ for the cases in Figure 7. For such high Reynolds numbers,

the viscous dissipation is evidently negligible and the early stage is characterized as "inviscid" or "kinematic". In the following stage, the droplet has been extensively spread out, and the significantly reduced droplet velocity results in much smaller *Re* and therefore significant viscous effects. Consequently, the difference in viscosity begins to affect the spreading process.

At *We*≈13, the droplet at *Oh*=0.0070 spreads faster but reaches β_{max} at a later time, which is consistent with the non-monotonic effects of viscosity on t_a as presented in Figure 3. The spreading diameter β of the droplet at *Oh*=0.0038 significantly decreases after reaching its β_{max}. For droplets at *Oh*=0.0070 and *Oh*=0.0592, the increased viscosity makes the droplets harder to retract than the droplet at *Oh*=0.0038.

Figure 8 shows the normalized height of droplet center h_c* (h_c*=h_c/D_0) as a function of normalized time τ at different *We* and *Oh*. It is noted that there is barely any difference for glycerol solution with varied viscosity and *We*, even for glycerol solution of *Oh*=0.0070 at *We*≈400 which splashes. The correlation of central height h_c* proposed by Roisman et al. (2009) can well predict the present experimental data for τ<0.4, when the droplet impact is in "*the first non-viscous regime*" characterized by h_c*=1-τ (Roisman et al., 2009). However there is some deviation of "*the second non-viscous regime*" characterized by h_c*=0.39(0.25+τ)$^{-2}$ from the present experimental data for τ>0.7. It is also noted that the time instant $\tau_{viscous}$, which indicates the beginning of "*the third viscous regime*" is undetermined in Roisman et al. (2009)'s model. Lagubeau et al. (2012) also proposed three regimes about the height of the droplet center. The model is same with that of Roisman et al. (2009) in "*pressure impact regime* (τ<0.5)" and similar in "*self-similar inertial regime* (0.5<τ< τ_p)". By using this model, the beginning of "*Plateau regime* (τ_p < τ)" as τ_p is approximately 3.3 for the droplet at *Oh*=0.0038 and *We*=13, which indicates that the data presented in Figure 8 is in the first and second regime.

4.2 Maximum spreading diameter and oscillation of droplets

Figure 9 shows the effect of Oh on β_{max} for different ranges of We. At relatively low We, β_{max} changes non-monotonically with increasing Oh. At $We\approx13$, β_{max} first increases from 1.92 for the droplet at Oh=0.0038 to 2.28 for the droplet at Oh=0.0070. After that, β_{max} decreases just as the tendency at higher We and ends with 1.55 for droplet at Oh=0.0592. At $We\approx30$, β_{max} also changes non-monotonically with the increase of viscosity with the peak at Oh=0.0070. This non-monotonic variation of $\beta_{\max}$ with viscosity has not been reported in the literature and is highly repeatable by conducting the experiment for many times and many new patches of glycerol solution. At intermediate We, although the disturbance at the rim is influenced non-monotonically by viscosity, the β_{max} still simply decreases with increasing Oh as shown at $We\approx60$,100 and 200 in Figure 9. At higher We ($We\approx400$) for the cases with Oh=0.0052, 0.0070, 0.0104, 0.0166 and 0.0287, the droplet keeps spreading after the thin-sheet breaks up and generates secondary droplets. The remaining part of the edge is still smooth and kept spreading, so we use the hollow dots to present β_{max} of the splashing cases, which is also decreased with the increase of viscosity.

Oscillating process of the droplet after contacting the surface has been presented and described in Figure 3. Since higher impact velocity reduced the amplitude of oscillations as illustrated by Banks et al. (2014), such phenomena is only observed for glycerol solution at quite small We ($We\approx13$ and 30). Figure 10a shows the non-dimensional the height of the apex at t_a, $H_a^*=H_a/D_0$ for different proportion of glycerol solution. Figure 10b shows the non-dimensional time t_a^* when the droplet reaches the first apex of oscillation, $t_a^*=t_aU_0/D_0$ for different proportion of glycerol solution.

5. Correlations on predicting β_{max}

5.1 Descriptions of Previous Models

In previous studies, there are three approaches for β_{max} correlation: scaling law, energy conservation, and momentum conservation, as summarized in Table 2. In the approaches based on

scaling law, a large number of data under different conditions with various liquids are used in order to get the model which fits other experiments. The scaling law of $\beta_{max} \sim (Re^2Oh)$ is used by Bayer and Megaridis (2006), Seo et al. (2015) and others. Laan et al. (2014) successfully described their data by a model using the Padé approximation. Lee et al. (2016b) modified the model of Laan et al. (2014) by introducing the non-dimensional maximum spreading diameter of the droplet impacting the surface at the vanishing velocity. Clanet et al. (2004) proposed different models for liquids at viscous and capillary regime.

In an approach based on momentum conservation, Roisman (2009) studied the ~~description of the~~ viscous flow of the unstable laminar flow in the film during the droplet spreading process, and obtained the self-similar solution of the viscous flow satisfying the Navier-Stokes equation. Then he proposed a model of β_{max} by using the expression of the boundary layer thickness in the theoretical results.

In the approaches based on energy conservation, the kinetic energy E_{K1} and surface energy E_{S1} of the droplet before the impact are transformed into the surface energy E_{S2} and the viscous dissipation E_{diss} after the droplet impacts the surface and reaches β_{max}, rendering the energy conservation equation $E_{k1}+E_{S1}=E_{diss}+E_{S2}$. E_{k1} and E_{S1} are usually calculated by $\pi/12\rho U_0^2 D_0^3$ and $\pi D_0^2\sigma$, respectively. For the surface energy at β_{max}, most of the previous studies assume $E_{S2}=0.25\pi D_{\max}^2\sigma$. The viscous dissipation term E_{diss} typically scales as $\Gamma\Omega t_{max}$, where Γ is the mean value of the viscous dissipation energy per unit time and volume, Ω is the volume where viscous dissipation occurs, and t_{max} is the time at the maximum spreading diameter. Γ and Ω is often assumed to be $\mu(U_0/\delta)^2$ and $\pi/4D_{\max}^2\delta$, respectively, where δ is the boundary layer thickness.

The prediction for t_{max} is very different in various models. Chandra and Avedisian (1991) assumed that $t_{max}=D_0/U_0$ as the time for the droplet height h going from its maximum value of D_0 to 0 at velocity U_0. Pasandideh‐Fard et al. (1996) modified t_{max} by estimating velocity at the edge of the splat during spreading V_R based on mass conservation and get $t_{max}=8/3D_0/U_0$. Lee et al. (2016a) assumed that t_{max}

scales with D_{max}/V_i instead of with D_0/V_i, and proposed $t_{max}=(\sigma_{liquid}/\sigma_{water})\ D_{max}/V_0$. Wildeman et al. (2016) found that $t_{max}=(\beta_{max}-1)D_0/U_0$ fitted their simulation data quite well. Lin et al. (2018) successfully collapsed all the experimental data into one curve by normalizing the spreading time with the modified capillary-inertial time and obtained $t_{max}=0.92We^{-0.43}\ (\rho R^3_{max}/\sigma)^{0.5}$. Wildeman et al. (2016) conducted numerical and theoretical studies on energy dissipation during the spreading and found that approximately half of the kinetic energy is converted to surface energy, being independent of the detailed parameters of the collision parameters and energy losses for high-impact wall velocities and collisions. Their model assumed the total dissipation E_{diss} includes the dissipation in the boundary layer E_d^{BL} and the head loss E_d^H, $E_{diss}=E_d^H+E_d^{BL}$, and E_d^H is equals to half of the initial kinetic energy according to the "1/2 rule".

5.2 Predictions of Previous Models

Figure 11 presents normalized measured time τ_{max} of droplets with varied *We* and *Oh,* and is compared with normalized measured time τ_{max} from some of above mentioned models. Apparently, τ_{max} is significantly reduced at higher impact velocity U_0 as indicated by the previous models. Chandra and Avedisian (1991) and Pasandideh‐Fard et al. (1996)'s models do not account for the effect of viscosity, which is manifest in the present experimental data. The τ_{max} also changes non-monotonically with the increase of viscosity as well as β_{max} and H_a*. Lin et al. (2018) and Wildeman et al. (2016)'s models can reflect the effect of viscosity to a certain extent, but have some deviations compared with the present experimental data. It can be seen that, for the models based on energy conservation, τ_{max} needs to be further improved for estimating the viscous dissipation during the droplet spreading.

Figure 12 presents the empirical fitting of β_{max} of droplets at different *Oh* based on several models at *We*≈13, 200 and 400. At *We*≈13, none of the models can exactly capture the non-monotonic change of β_{max} with the increasing *Oh*. At *We*≈200, both Lee et al. (2016b) and Wildeman et al. (2016)'s model

show good prediction of β_{max} for glycerol solution with different viscosity. At $We\approx400$, the β_{max} of splashing cases are presented by measuring the smooth edge of the remaining part of the droplet after splashing, it's noted that Lee et al. (2016b) and Wildeman et al. (2016)'s models still predicted β_{max} well.

Figure 13 shows the deviations of the predictions from different models on β_{max}. Models based on energy conservation are shown in Figure 13a, and models based on scaling law or momentum conservation are presented in Figure 13b. The deviation is calculated by $\sum_{i=1}^{n}\left|\beta^{i}_{max\_exp}-\beta^{i}_{max\_model}\right|/n$ for droplet with n data points. Most of the models based on scaling law is clearly restricted by the liquid used in the original model. Seo et al. (2015)'s model is based on ethanol, isooctane and gasoline, which all have small surface tension, doesn't fit the data of glycerol solution well and has the deviation of larger than 12%. Lin et al. (2018) proposed four reasons why most models based on mass and momentum conservation are inaccurate, which still apply to following models and explained why some models do not fit well with glycerol solution. Among these models, the model of Wildeman et al. (2016) and Lee et al. (2016b) fit the experimental values with smallest deviation which is less than 5%. We note that at small *We* cases, all models in Table 2 do not qualitatively predict the non-monotonic dependence of $\beta_{\max}$ on *Oh*, so the data set at $We\approx13$ and 30 are not included Figure 13.

5.3 Theoretical Considerations for Future Modelling

The model of Wildeman et al. (2016) fits our experimental data with a mean error being less than 5% for $We>30$. Wildeman et al. also numerically demonstrated that their model, especially the "1/2 rule", is only suitable for $We>30$. This results in the relatively large deviation of the model from the present experimental data at $We\approx13$, as shown in Figure 12a. For future modelling efforts, some theoretical considerations are presented in the following.

The difficulty of establishing a predicting model for droplet spreading below We≈30 roots in the absence of an asymptotically accurate model for droplet shape. As the Weber number increases from 0 to 30, the droplet shape (at the instant of maximum spreading) resembles from a spherical cap, to a puddle with a flattened top, and to a doughnut (Wildeman et al., 2016). The great success of previous models for droplet spreading at higher Weber number is largely owing to the existence of fairly precise "pizza" model for the droplet shape − a thin, almost flat central part bordered by a thick cylindrical rim (Wildeman et al., 2016).

Another important feature of droplet impact below We≈30 is the substantial amount of "left-over" kinetic energy in the form of vortical flow. This energy is comparably negligible in the energy budget at higher Weber numbers and therefore is not taken into account in previous models. The existence of the "left-over" kinetic energy is manifested by the oscillation of droplet at its maximum spreading, as seen in Figure 10. Bearing this in mind, we examined each term in the model of Wildeman et al. (2016), which can be rewritten in the present nomenclature by

$$\frac{12}{We}+\frac{1}{2}=\frac{3(1-cos\theta)}{We}\beta_m^2+\frac{\alpha}{\sqrt{Re}}\beta_m^2\sqrt{\beta_m-1} \qquad (1)$$

where each term from left to right represents the initial surface energy (normalized by the initial kinetic energy), the "1/2" of initial kinetic energy entering the energy budget (the other half is a geometric head loss), the surface energy at the maximum spreading, and the total viscous dissipation.

As an attempt to extend Wildeman et al.'s model to lower Weber numbers, we proposed to replace its kinetic energy term, i.e. "1/2", by a factor of $f(We, Oh)$ to account for the significant "left-over" kinetic energy. Therefore, we have

$$\frac{12}{We}+f(We,Oh)=\frac{3(1-cos\theta)}{We}\beta_m^2+\frac{\alpha}{\sqrt{Re}}\beta_m^2\sqrt{\beta_m-1} \qquad (2)$$

where the factor should asymptotically approach to 1/2 for We>30 as stated in Wildeman et al. (2016). The factor $f(We, Oh)$ by fitting the present experimental data into the above form is presented in Figure 14. It's noted that for droplets at We>30, $f(We, Oh)$ is around 0.5 as it should be. At We≈13, $f(We$=13,

Oh) is 0.1, 0.3 and 0.7 for *Oh*=0.0038, 0.0052 and 0.0070 respectively. At *We*≈30, *f* (*We*=30, *Oh*) is 0.2, 0.5 and 0.6 for *Oh*=0.0038, 0.0052 and 0.0070 respectively. The non-monotonic variation of *f* (*We*, *Oh*) with *Oh* is somewhat consistent with the non-monotonic variation of droplet oscillation with *Oh*, which has been shown in Figure 10.

The role of liquid viscosity in suppressing droplet spreading has been well recognized through the viscous dissipation mechanism. Consequently, most of the previous models, which have taken into account of viscosity effect, imply a monotonically increasing function of *Oh*. This can be understood by the fact that, for droplet impact with large impact inertia, the droplet internal flow during spreading is dominantly controlled by the conversion of kinetic energy to surface energy, which is quantified by using *We*; the concomitant viscous dissipation is merely a "passive scalar" quantified by using *Re* or *Oh*. Modelling such a viscous effect in an energy conservation analysis can be done by estimating the viscous dissipation rate $\Phi = \mu f(\dot{\gamma})$, which is a monotonic increasing function of μ; $\dot{\gamma} = g(We)$ is the characteristic strain rate of the droplet internal flow and depends only on *We*. The monotonic dependence of Φ on either *Re* or *Oh* are evident, for example, the last term on the RHS of Equation (1). The accuracy of such estimation relies on the sophistication of modelling the two functions *f* and g, which in turn reply on the accuracy of modelling droplet shape.

As we discussed above, an asymptotically accurate model for droplet deformation at small *We* may not exist. This also adds difficulty to modelling viscous dissipation. Unlike the situation at high *We*, the droplet spreading flow at small *We* is strongly affected by the viscous stress. Consequently, another role of liquid viscosity may manifest itself through its influence on modulating the droplet internal flow at small *We*s. The above approximation $\dot{\gamma} = g(We)$ may have to be replaced by $\dot{\gamma} = g'(We,\mu)$, which could be a monotonically decreasing function of μ.

Based on the above albeit discussions, a quantitively predictive model for the presently observed non-monotonic droplet spreading is unavailable in the present study, because it needs not only more

accurate experimental data for We<30 but also the help of numerical simulation for quantifying the droplet shape and the droplet internal flow, which will be considered in our future work.

6. Conclusion

A comprehensive experimental study on a droplet with different viscosity (characterized by dimensionless Ohnesorge number, Oh) impacting on a smooth surface is presented in the paper, which emphasizes on clarifying the effects of viscosity on spreading process. The most interesting experimental observation in the present study, which was not reported in the literature or captured by the previous models, is that, at relatively small Weber number (We<30), the maximum spreading diameter β_{max} of droplet first increases and then decreases with increasing Oh, showing non-monotonic tendency with the increasing viscosity. At higher Weber numbers (We>30), the present results show a good agreement with the previous experimental data and model predictions.

A qualitative explanation to the above observations is as follows. The droplet deformation (including spreading) and the internal flow are not dominantly controlled by impact inertia at smaller We, in which the liquid viscosity plays important, "active" roles. First, the previously neglected "left-over" kinetic energy was found significant at small We and vary with Oh (or Re) (Wildeman et al. 2016). Second, the droplet shape at the maximum spreading appears complex morphological change, on which the viscous effects have not been fully understood. Third, the reduction of flow strain rates by increasing viscosity could be more prominent than the increase of dissipation coefficient. All of these pose great challenge to modelling droplet spreading at small We.

At relatively high Weber number, the droplet spreading and the flow strain rates are increasingly controlled by the impact inertia and the viscosity tends to play the "passive" role as the maximum spreading diameter decreases with increasing the viscosity. However, some unsmooth disturbance around the rim occurs only at intermediate Oh. At even higher Weber number, the impact outcome transits from deposition to splashing and to deposition again with the increase of viscosity, implies

another dual role of viscosity at relatively high Weber number. All these non-monotonic ~~spreading~~ behaviors reflect the dual role of liquid viscosity, which certainly requires ~~future~~ more experimental and numerical work in the future.

Acknowledgement

The work at Xi'an Jiaotong University was supported by the National Natural Science Foundation of China (51722603, and 91541107), the Fundamental Research Funds for the Central Universities, Science Challenging Program (TZ201601), and the State Key Laboratory of Engines (K2018-14). The work at the Hong Kong Polytechnic University was supported by the Hong Kong Research Grants Council/General Research Fund (PolyU 152217/14E and PolyU 152651/16E) and partly by Central Research Grant (G-SB1Q).

References

Allen, R.F., 1975. The role of surface tension in splashing. Journal of Colloid & Interface Science 51, 350-351.
Banks, D., Ajawara, C., Sanchez, R., Surti, H., Aguilar, G., 2014. Effects of liquid and surface characteristics on oscillation behavior of droplets upon impact. Atomization & Sprays 24, 895-913.
Bayer, I.S., Megaridis, C.M., 2006. Contact angle dynamics in droplets impacting on flat surfaces with different wetting characteristics. Journal of Fluid Mechanics 558, 415-449.
Bhola, R., Chandra, S., 1999. Parameters controlling solidification of molten wax droplets falling on a solid surface. Journal of Materials Science 34, 4883-4894.
Chandra, S., Avedisian, C.T., 1991. On the Collision of a Droplet with a Solid Surface. Proceedings of the Royal Society A: Mathematical, Physical and Engineering Sciences 432, 13-41.
Clanet, C., BÉGuin, C., Richard, D., QuÉRÉ, D., 2004. Maximal deformation of an impacting drop. Journal of Fluid Mechanics 517, 199-208.
de Ruiter, J., Pepper, R.E., Stone, H.A., 2010. Thickness of the rim of an expanding lamella near the splash threshold. Physics of Fluids 22, 022104.
Driscoll, M.M., Nagel, S.R., 2011. Ultrafast interference imaging of air in splashing dynamics. Phys Rev Lett 107, 154502.
Gao, S., Liao, Q., Liu, W., Liu, Z., 2018. Nanodroplets Impact on Rough Surfaces: A Simulation and Theoretical Study. Langmuir : the ACS journal of surfaces and colloids 34, 5910-5917.
Hulse-Smith, L., Mehdizadeh, N.Z., Chandra, S., 2005. Deducing drop size and impact velocity from circular bloodstains. Journal of Forensic Sciences 50, 54-63.
Josserand, C., Thoroddsen, S.T., 2016. Drop Impact on a Solid Surface. Annual Review of Fluid Mechanics 48, 365-391.
Joung, Y.S., Buie, C.R., 2015. Aerosol generation by raindrop impact on soil. Nature communications 6, 9.
Laan, N., de Bruin, K.G., Bartolo, D., Josserand, C., Bonn, D., 2014. Maximum Diameter of Impacting Liquid Droplets. Physical Review Applied 2, 044018.
Lagubeau, G., Fontelos, M.A., Josserand, C., Maurel, A., Pagneux, V., Petitjeans, P., 2012. Spreading dynamics of drop impacts. Journal of Fluid Mechanics 713, 50-60.
Lee, J.B., Derome, D., Guyer, R., Carmeliet, J., 2016a. Modeling the Maximum Spreading of Liquid Droplets

Impacting Wetting and Nonwetting Surfaces. Langmuir : the ACS journal of surfaces and colloids 32, 1299-1308.
Lee, J.B., Laan, N., de Bruin, K.G., Skantzaris, G., Shahidzadeh, N., Derome, D., Carmeliet, J., Bonn, D., 2016b. Universal rescaling of drop impact on smooth and rough surfaces. Journal of Fluid Mechanics 786, R4.
Lin, S.J., Zhao, B.Y., Zou, S., Guo, J.W., Wei, Z., Chen, L.Q., 2018. Impact of viscous droplets on different wettable surfaces: Impact phenomena, the maximum spreading factor, spreading time and post-impact oscillation. Journal Of Colloid And Interface Science 516, 86-97.
Martin, G.D., Hoath, S.D., Hutchings, I.M., Iop, 2008. Inkjet printing - the physics of manipulating liquid jets and drops, Engineering And Physics - Synergy for Success. Iop Publishing Ltd, Bristol.
Matas, J.P., 2015. Inviscid vs viscous instability mechanism of an air-water mixing layer. Journal of Fluid Mechanics 768, 375-387.
Moreira, A.L.N., Moita, A.S., Panão, M.R., 2010. Advances and challenges in explaining fuel spray impingement: How much of single droplet impact research is useful? Progress in Energy and Combustion Science 36, 554-580.
Mundo, C., Sommerfeld, M., Tropea, C., 1995. Droplet-wall collisions: Experimental studies of the deformation and breakup process. International Journal of Multiphase Flow 21, 151-173.
Naraigh, L.O., Spelt, P.D.M., 2018. Instability of pressure-driven gas-liquid two-layer channel flows in two and three dimensions. Journal Of Fluid Mechanics 849, 1-34.
Pasandideh‐Fard, M., Qiao, Y.M., Chandra, S., Mostaghimi, J., 1996. Capillary effects during droplet impact on a solid surface. Physics of Fluids 8, 650-659.
Range, K., Feuillebois, F., 1998. Influence of Surface Roughness on Liquid Drop Impact. Journal of Colloid and Interface Science 203, 16-30.
Rioboo, R., Marengo, M., Tropea, C., 2001. Outcomes from a Drop Impact on Solid Surfaces. Atomization & Sprays 11, 155-166.
Rioboo, R., Marengo, M., Tropea, C., 2002. Time evolution of liquid drop impact onto solid, dry surfaces. Experiments in Fluids 33, 112-124.
Roisman, I.V., 2009. Inertia dominated drop collisions. II. An analytical solution of the Navier–Stokes equations for a spreading viscous film. Physics of Fluids 21, 052104.
Roisman, I.V., Berberović, E., Tropea, C., 2009. Inertia dominated drop collisions. I. On the universal flow in the lamella. Physics of Fluids 21, 052103.
Scheller, B.L., Bousfield, D.W., 1995. Newtonian Drop Impact with Solid Surface. Aiche Journal 41, 1357-1367.
Seo, J., Lee, J.S., Kim, H.Y., Yoon, S.S., 2015. Empirical model for the maximum spreading diameter of low-viscosity droplets on a dry wall. Experimental Thermal and Fluid Science 61, 121-129.
Smith, F.R., Buntsma, N.C., Brutin, D., 2018. Roughness Influence on Human Blood Drop Spreading and Splashing. Langmuir : the ACS journal of surfaces and colloids 34, 1143-1150.
Stow, C.D., Hadfield, M.G., 1981. An Experimental Investigation of Fluid Flow Resulting from the Impact of a Water Drop with an Unyielding Dry Surface. Proceedings of the Royal Society of London 373, 419-441.
Tang, C., Qin, M., Weng, X., Zhang, X., Zhang, P., Li, J., Huang, Z., 2017. Dynamics of droplet impact on solid surface with different roughness. International Journal of Multiphase Flow 96, 56-69.
Thoroddsen, S.T., Sakakibara, J., 1998. Evolution of the fingering pattern of an impacting drop. Physics of Fluids 10, 1359-1374.
Ukiwe, C., Kwok, D.Y., 2005. On the maximum spreading diameter of impacting droplets on well-prepared solid surfaces. Langmuir the Acs Journal of Surfaces & Colloids 21, 666-673.
Vadillo, D.C., Soucemarianadin, A., Delattre, C., Roux, D.C.D., 2009. Dynamic contact angle effects onto the maximum drop impact spreading on solid surfaces. Physics of Fluids 21, 122002.
Vu, H., Banks, D., Aguilar, G., 2011. Examining viscosity and surface wettability on lamella lift dynamics and droplet splashing. Atomization & Sprays 21, 303-315.
Wang, Y., Dandekar, R., Bustos, N., Poulain, S., Bourouiba, L., 2018. Universal Rim Thickness in Unsteady Sheet Fragmentation. Physical Review Letters 120, 204503.
Wildeman, S., Visser, C.W., Sun, C., Lohse, D., 2016. On the spreading of impacting drops. Journal of Fluid Mechanics 805, 636-655.
Xu, L., Zhang, W.W., Nagel, S.R., 2005. Drop splashing on a dry smooth surface. Phys Rev Lett 94, 184505.
Yarin, A.L., 2006. Drop impact dynamics: splashing, spreading, receding, bouncing…. Annual Review of Fluid

Mechanics 38, 159-192.
Zhang, B., Li, J., Guo, P., Lv, Q., 2017. Experimental studies on the effect of Reynolds and Weber numbers on the impact forces of low-speed droplets colliding with a solid surface. Experiments in Fluids 58, 125.

List of Figure captions

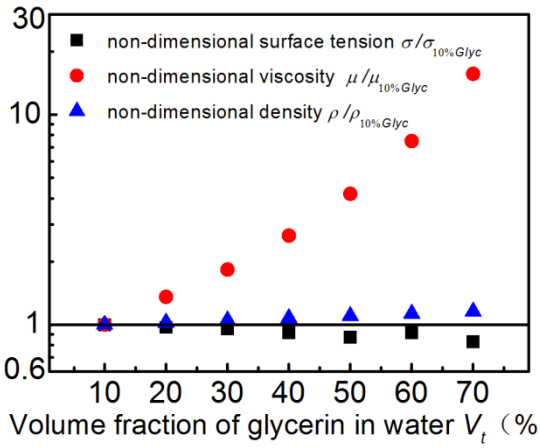

Figure 1 Non-dimensional surface tension, viscosity and density of experimental liquids

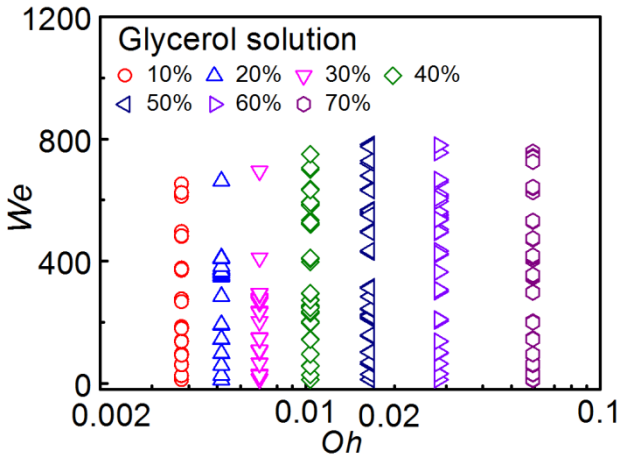

Figure 2 Test ranges of non-dimensional parameters *Oh* and *We*

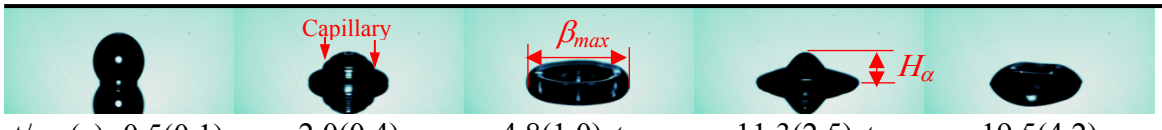

t/ms(τ)=0.5(0.1)	2.0(0.4)	4.8(1.0)-t_{max}	11.3(2.5)-t_a	19.5(4.2)	*Oh*=0.0038
23.6(5.1)	29.9(6.5)	35.3(7.7)	39.4(8.6)	43.5(9.4)	
t/ms(τ)=0.5(0.1)	2(0.5)	5.2(1.2)-t_{max}	15(3.5)-t_a	20(4.7)	*Oh*=0.0070
t/ms(τ)=0.5(0.1)	2(0.4)	3.2(0.7)-t_{max}	9.3(2.0)- t_a	Cap shape at equilibrium 20(4.3)	*Oh*=0.0592

Figure 3 Impact, spreading and oscillation of droplets at *We*≈13 and different *Oh*.

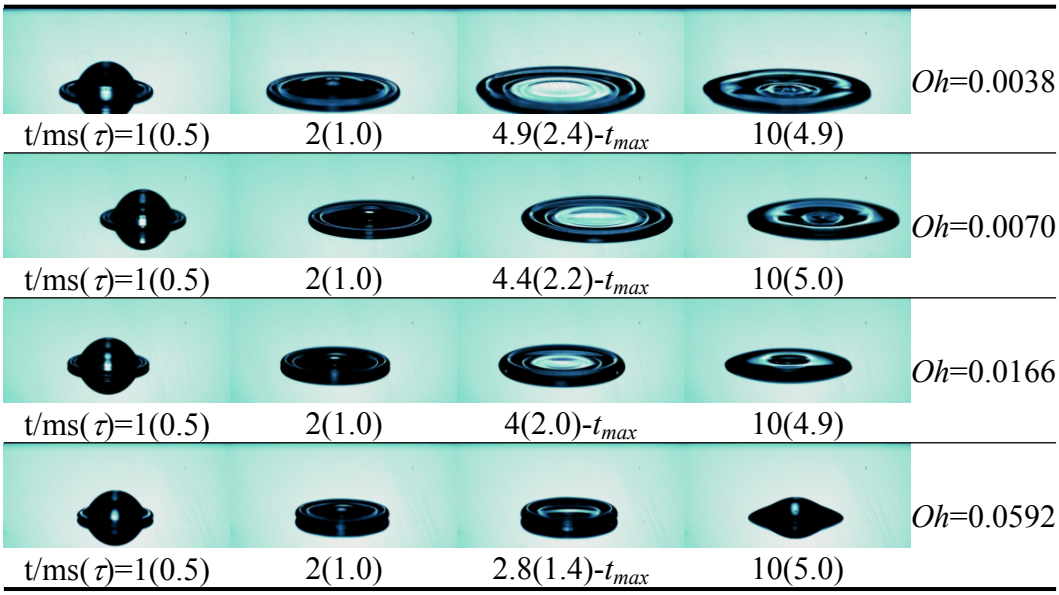

t/ms(τ)=1(0.5)	2(1.0)	4.9(2.4)-t_{max}	10(4.9)	*Oh*=0.0038
t/ms(τ)=1(0.5)	2(1.0)	4.4(2.2)-t_{max}	10(5.0)	*Oh*=0.0070
t/ms(τ)=1(0.5)	2(1.0)	4(2.0)-t_{max}	10(4.9)	*Oh*=0.0166
t/ms(τ)=1(0.5)	2(1.0)	2.8(1.4)-t_{max}	10(5.0)	*Oh*=0.0592

Figure 4 Impact and spreading of droplets at *We*≈60 and different *Oh*.

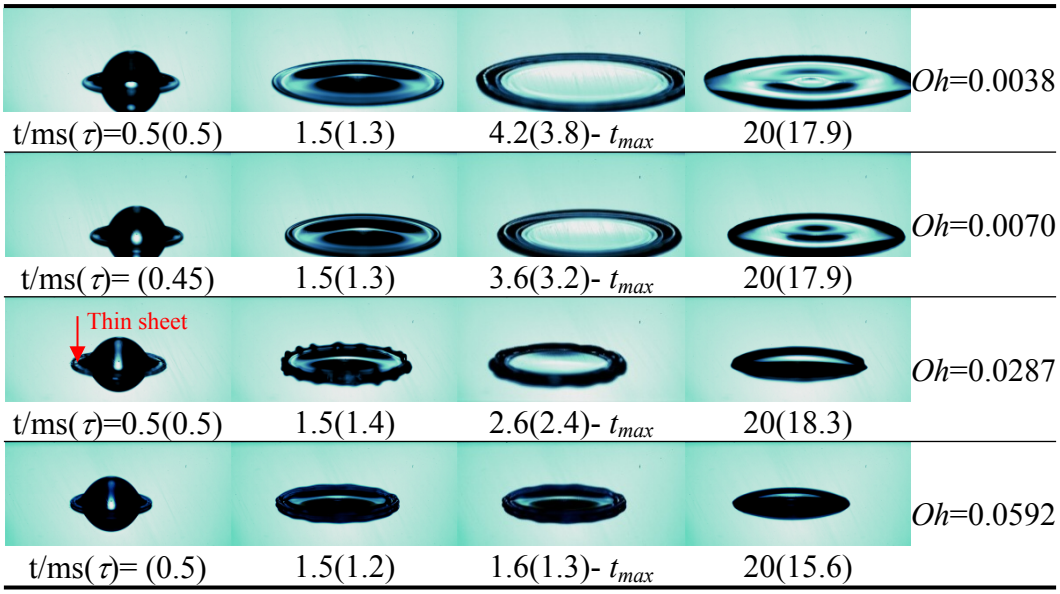

(a)Images at different time

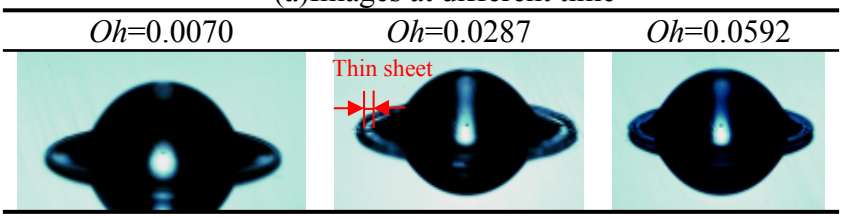

(b)Partially enlarged images at t=0.5ms at different *Oh*

Figure 5 Impact, spreading and thin-sheet instability of droplets at *We*≈200 and different *Oh*.

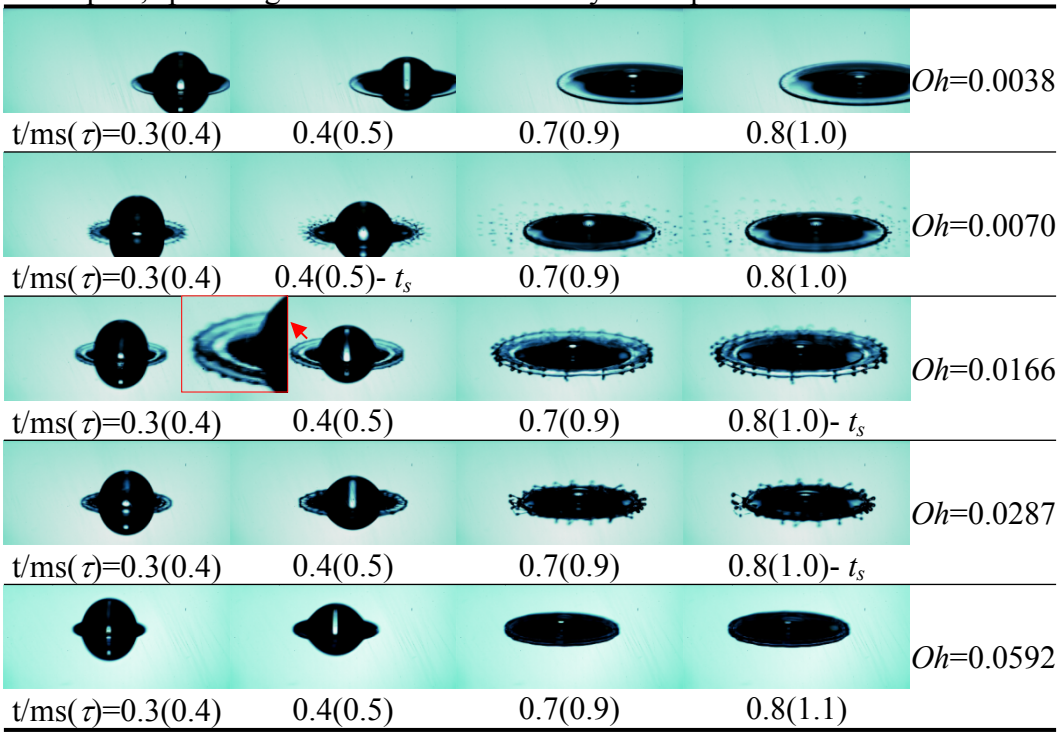

Figure 6 Impact, spreading and splashing of droplets at *We*≈400 and different *Oh*.

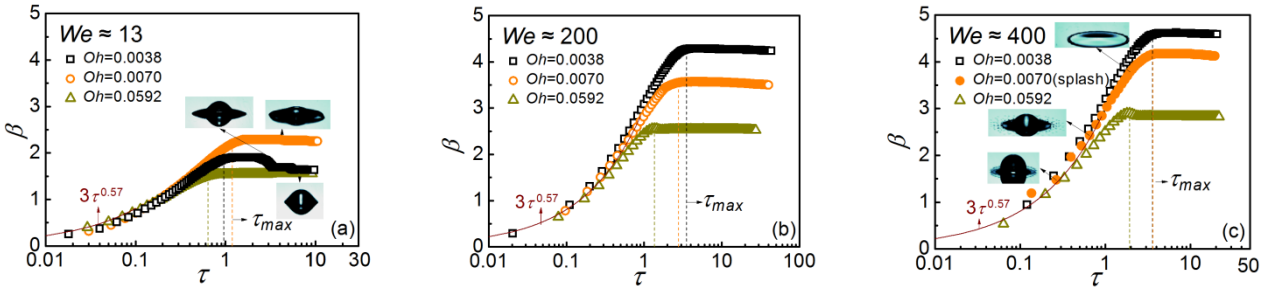

Figure 7 Evolution of normalized spreading diameter β at different *We* and *Oh*.

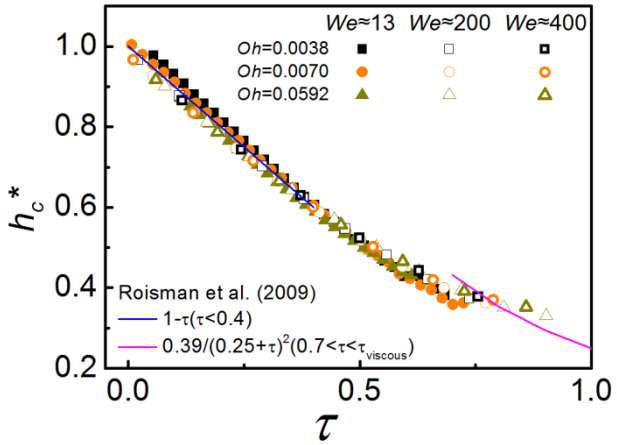

Figure 8 Evolution of normalized height of droplet center at different *We* and *Oh*.

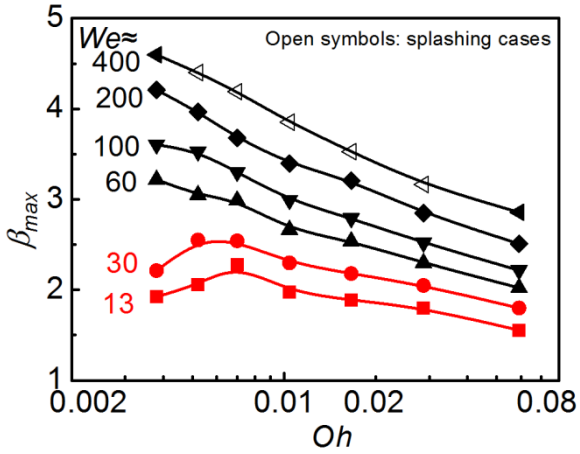

Figure 9 β_{max} of glycerol solution with varied viscosity at different *We*

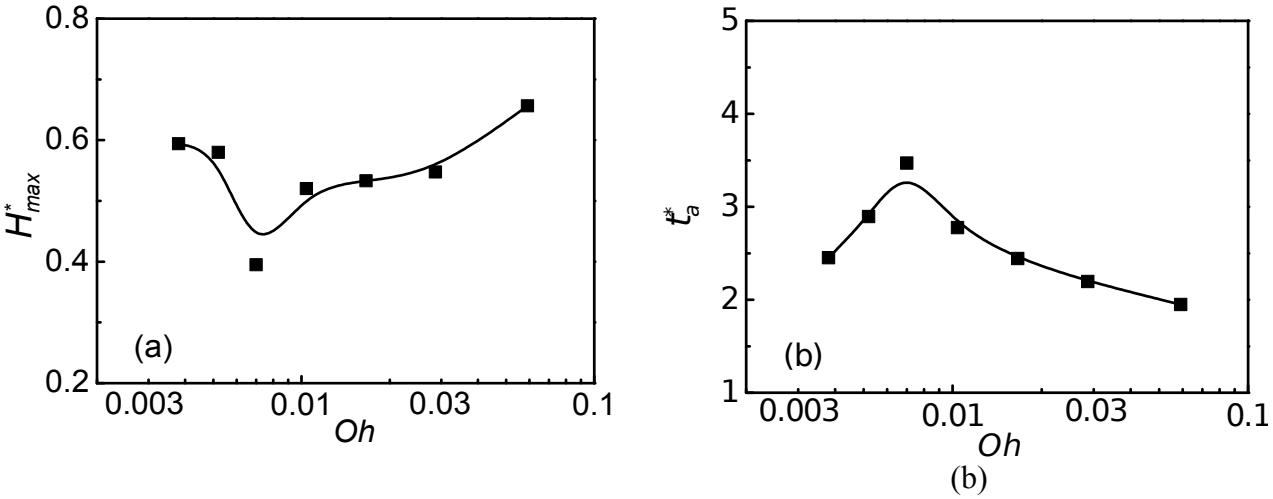

Figure 10 Dimensionless parameters of oscillation of glycerol solution with varied *Oh at We*≈13

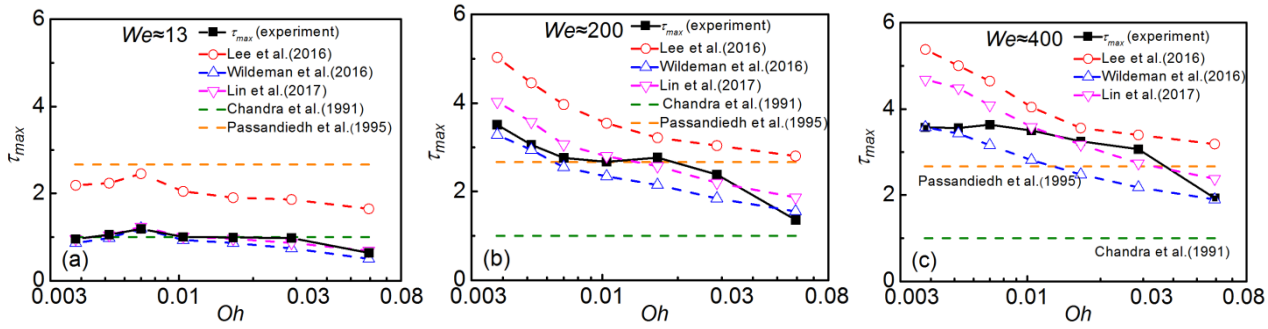

Figure 11 Comparison of measured spreading time τ_{max} and empirical fitting of models

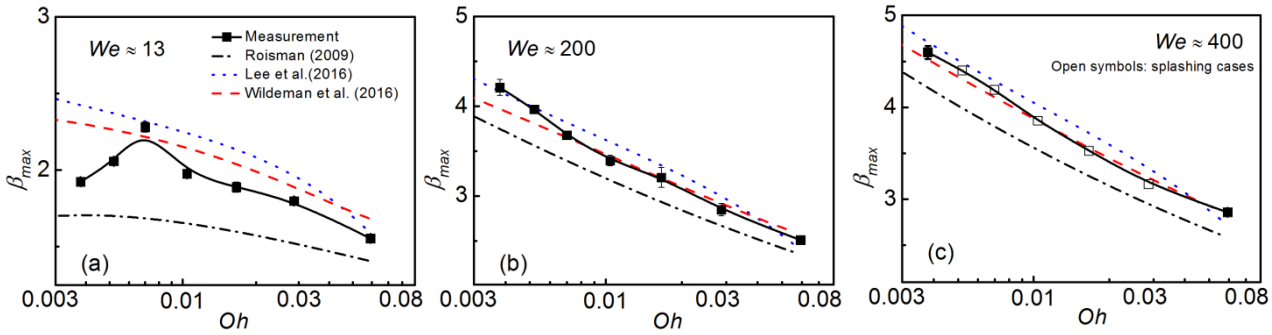

Figure 12 Empirical correlation comparison of different models on predicting β_{max}

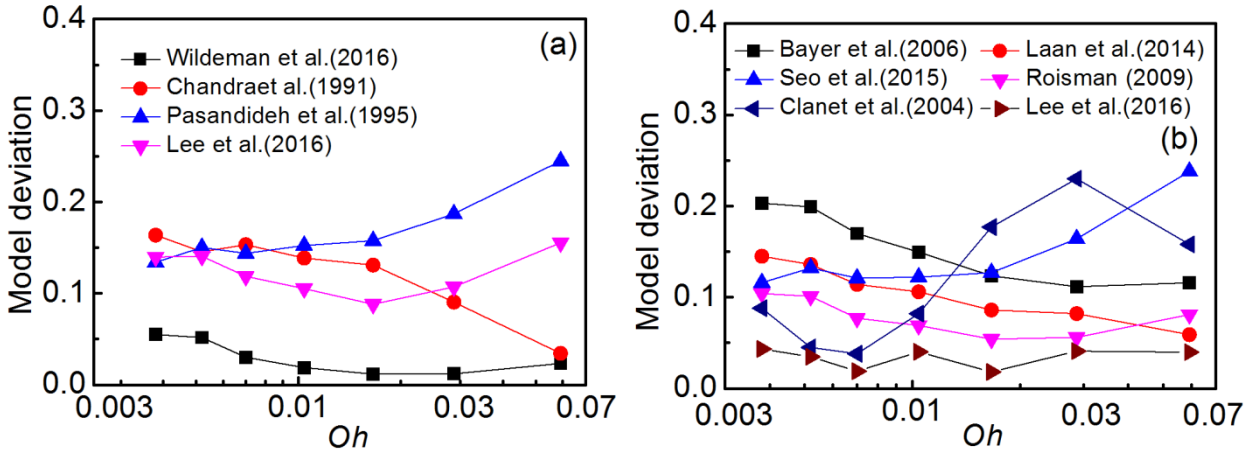

Figure 13 Mean error of the fitting based on different models with experimental $\beta_{max;}$
The data set for small Weber number case (We<30) is not included.

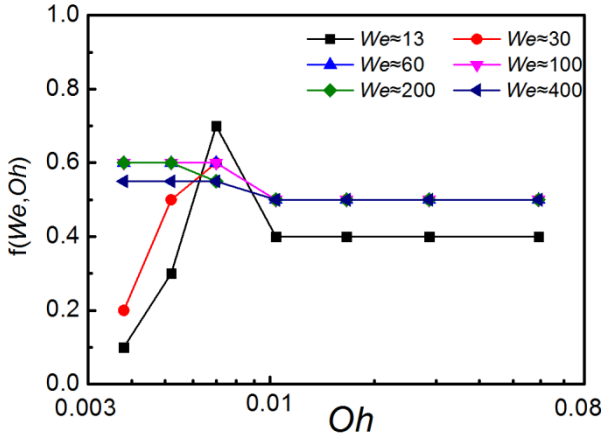

Figure 14. The "left-over kinetic energy" factor $f(We, Oh)$ by fitting the present experimental data.

List of Table captions

Table 1 Physical properties of liquid droplets at 1 atm and 20 ℃

Liquid	*Oh*	Surface tension (N/m)	Viscosity (mPa·s)	Density (g/cm^3)	Diameter (mm)
10% glycerol solution	0.0038	0.070	1.60	1.020	2.52±0.07
20% glycerol solution	0.0052	0.068	2.17	1.045	2.50±0.03
30% glycerol solution	0.0070	0.067	2.93	1.070	2.48±0.03
40% glycerol solution	0.0104	0.064	4.25	1.097	2.43±0.03
50% glycerol solution	0.0166	0.061	6.72	1.123	2.39±0.03
60% glycerol solution	0.0287	0.064	12.00	1.151	2.37±0.03
70% glycerol solution	0.0592	0.058	25.08	1.178	2.31±0.03

Table 2 Previous empirical models regarding the maximum spreading diameter

Methods	**Refs.**	**Droplet-solid surface**	**β_{max} equation**
Scaling law	Scheller et al. (1995)	Glycerin-water-ethanol droplet, smooth polystyrene film/glass	$\beta_{max}=0.61(We/Oh)^{0.166}$
	Clanet et al. (2004)	Water and mercury droplet, smooth super-hydrophobic surface	$\beta_{max}\sim We^{0.25}$ for $(We/Re^{4/5})<1$ $\beta_{max}\sim \mathrm{Re}^{0.2}$ for $(We/Re^{4/5})>=1$
	Bayer et al. (2006)	Water droplet, smooth polished stainless steel surface	$\beta_{max}=0.72(We/Oh)^{0.14}$
	Laan et al. (2014)	Water with/without glycerol, blood droplet, smooth stainless steel surface	$\beta_{max}=Re^{1/5}\mathrm{P}^{1/2}/(\mathrm{A}+\mathrm{P}^{1/2})$，$\mathrm{P}=WeRe^{-2/5}$，$\mathrm{A}=1.24\pm0.01$
	Seo et al. (2015)	Gasoline, isooctane, ethanol, smooth aluminum surface	$\beta_{max}=1.72(We_x/Oh_x)^{0.122}(\mu_{iso}\sigma_{iso}/\mu_x\sigma_x)$, corrected by the physical properties fluids
	Lee et al. (2016)	Water/ethanol/glycerol solution droplet, Surfaces with varied roughness and contact angle	$(\beta^2_{max}-\beta^2_{Vi\to0})^{1/2}Re^{-1/5}=We^{1/2}/(\mathrm{A}+We^{1/2})$, A=7.6
Energy conservation	Pasandideh et al. (1995)	Water with surfactants, polished stainless steel surface	$\beta_{max}=\sqrt{(We+12)/[3(1-\cos\theta_a)+4WeRe^{-0.5}]}$
	Ukiwe et al. (2005)	Water droplet, smooth polymer coated surface	$\beta_{max}^3\left(3(1-\cos\theta_Y)+4WeRe^{-0.5}\right)=(We+8)\beta_{max}-8$
	Sen et al. (2014)	Biofuel droplet, smooth stainless steel surface	$\sqrt{(We+12)/[3(1-\cos\theta_Y)+4WeRe^{-0.5}]}\sim 1.73We^{0.14}$
	Wildeman et al. (2016)	Water droplet, smooth surface	$\frac{3(1-\cos\theta)}{We}\beta_m^2+\frac{\alpha}{\sqrt{Re}}\beta_m^2\sqrt{\tilde{\beta}_m-1}=\frac{12}{We}+\frac{1}{2}$,no-slip, $We>30$
	Lee et al. (2016)	Ethanol/water/glycerol droplet, surfaces with varied roughness and contact angle	$We+12=3\beta^2_{max}(1-\cos\theta)+8/\beta_{max}+3(\sigma/2\sigma_{water})^{1/2}\beta^{5/2}_{max}We/Re^{1/2}$
Momentum conservation	Roisman (2009)	Water droplet, smooth surface with different contact angle	$\beta max\approx 0.87Re^{1/5}-0.40Re^{2/5}We^{-1/2}$